https://doi.org/10.1016/j.jmps.2017.11.026
This is the Pre-Published Version.

Edge orientations of mechanically exfoliated anisotropic two-dimensional materials

Juntan Yang[1], Yi Wang[2], Yinfeng Li[3], Yang Chai[2*], Haimin Yao[1*], Huajian Gao[4]

[1]Department of Mechanical Engineering, The Hong Kong Polytechnic University, Hung Hom, Kowloon, Hong Kong

[2]Department of Applied Physics, The Hong Kong Polytechnic University, Hung Hom, Kowloon, Hong Kong

[3]Department of Engineering Mechanics, Shanghai Jiao Tong University, Shanghai, China

[4]School of Engineering, Brown University, Providence, RI 02912, USA

Mechanical exfoliation is an approach widely utilized to prepare high-crystalline-quality two-dimensional (2D) materials for investigating their intrinsic physical properties. During mechanical exfoliation, in-plane cleavage results in new edges, whose orientations plays an important role in determining the properties of the as-exfoliated 2D materials especially for those with high anisotropy. Here, we systematically investigate the factors affecting the edge orientation of 2D materials created by mechanical exfoliation. Our theoretical study manifests that the preferred fractured direction during mechanical exfoliation is determined synergistically by tearing direction and anisotropy of fracture energy. This theory, in combination with the crystallographic structure of a specific 2D material, allows us to predict the possible edge orientation of mechanically exfoliated 2D materials as well as their probabilities of occurrence. The theoretical predication is indirectly verified by examining the inter-edge angles of the mechanically exfoliated 2D materials including graphene, MoS_2, PtS_2, and black phosphorous. This work not only sheds light on the mechanics of exfoliation of 2D materials, but also opens a new area of deriving information of edge orientations of mechanically exfoliated 2D materials by data mining of their macroscopic geometric features.

© 2017. This manuscript version is made available under the CC-BY-NC-ND 4.0 license https://creativecommons.org/licenses/by-nc-nd/4.0/

Introduction.—Two-dimensional (2D) materials refer to crystalline materials consisting of one or a few layers of atoms. Due to the ultrathin thickness and ultrahigh specific surface area, 2D materials exhibit distinctive properties that are absent in their bulk counterparts [1-4], showing great potentials for various applications [2,3,5-10]. A variety of physical and chemical approaches have been developed to acquire 2D materials [11-16]. Among them, mechanical exfoliation is the most facile one for producing 2D materials with high crystalline quality [1,16-18]. The size and shape of the 2D material flake obtained by mechanical exfoliation depend on a variety of factors, including the adhesion property of the tape, the crystalline structure and mechanical properties of the layered material. For example, preliminary experiments showed that the edges of a 2D material flake obtained by mechanical exfoliation exhibit distinctive crystallographic orientations [18-20]. The regular distribution patterns of the inter-edge angles imply that the fracture of the material during exfoliation process has some preferred directions even by random peeling processing.

It is of great value to understand the factors determining the crystal orientations of the exfoliated flakes for the prediction and manipulation of the anisotropy of 2D materials in their electrical [4,21-23], mechanical [24-26] and optical properties [20,27,28]. For example, it has been shown that the stretching along the armchair direction of monolayer MoS_2 can generate piezoelectric polarization charge on the zig-zag edges [22]. Prevalent methods to identify the crystallographic structure of 2D materials include transmission electron microscopy (TEM) [29,30] and second harmonic generation(SHG) [20,31,32], both of which involve costly facilities and time-consuming processes of sample preparation. A fast and non-destructive approach to identify the crystallographic orientations is still in great demand.

In this work, we develop a universal theoretical model based on fracture mechanics

to predict preferred fracture directions of 2D materials and their probabilities of occurrence. We collect a number of inter-edge angles of 2D flakes and perform statistical analysis, which is in good agreement with our theoretical predictions. More importantly, we reveal that the fracture direction of 2D materials is dependent on not only the tearing angle but also the edge energies of 2D materials, especially for those with high anisotropic properties. Although we validate this theoretical model with only 4 typical 2D materials, including graphene, MoS_2(2H), PtS_2(1T) and black phosphorous (BP), it can be also extended to the predication of other 2D materials and provide us fundamental understanding of the fracture process of 2D materials.

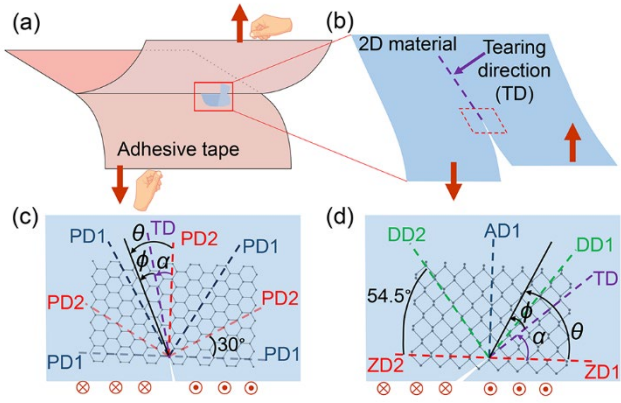

FIG. 1. (a) Schematics of mechanical exfoliation of 2D materials. (b) Schematic illustration of a cracking model describing the tearing process of 2D materials during exfoliation. (c-d) Closeup of the configuration near the crack tips of hexagonal and orthorhombic 2D materials under tearing. PD: Principal direction, TD: Tearing direction; AD: Armchair direction; ZD: Zigzag direction; DD: Diagonal direction.

Fracture direction of 2D materials during mechanical exfoliation.—Mechanical exfoliation of 2D materials is often carried out by the aid of sticky tapes such as scotch tape. A typical exfoliation process of graphene, for example, often starts from attaching a piece of pristine scotch tape onto a graphite wafer. Then, the tape is slowly peeled off from the graphite, bringing along with a few-layer graphene flake stuck to the tape. The tape with graphene flake is then stuck to another piece of pristine tape. After being

compressed for better contact, these two pieces of tape are then detached from each other slowly [see Fig. 1(a)]. By doing so, the graphene flake is split into two thinner parts. This process can be repeated until a monolayer graphene flake is acquired. Similar exfoliation procedure also applies to the other 2D materials such as MoS_2, PtS_2, and BP.

The flakes obtained by mechanical exfoliation exhibit polygonal shape with average size around a few microns. The straight-line segments along the polygonal edge imply their specific crystallographic orientations [18,33,34]. To predict the orientation of these edges that result from the tearing-induced cleavage, a theoretical model is proposed, in which a piece of cracked 2D material is torn by out-of-plane loadings, as schematically depicted in Fig. 1(b). For such tearing loading, classical linear elastic fracture mechanics (LEFM) indicates that the driving force for crack propagation can be quantified by the energy release rate (ERR) near the crack tip and exhibits directional dependence [35]

$$G(\phi)=\frac{G_0}{2}(1+\cos\phi) \tag{1}$$

where ϕ represents the direction angle relative to the line of the pre-existing crack [see Fig. 1(c)] and G_0 stands for the ERR at $\phi=0$. Clearly, G_0 is the maximum of $G(\phi)$. The direction along the line of the pre-existing crack is designated as *tearing direction* (TD). But it does not mean that the crack will necessarily propagate along the tearing direction, because the resistance of 2D materials against fracture, which is characterized by the fracture energy, may have directional dependence as well. Taking graphene as an example, it has been shown that its edge energy, which can be deemed as half of its fracture energy, exhibits strong directional dependence given by [36]

$$\gamma(\theta)=\frac{\gamma_1}{\sin\pi/6}\sin\theta+\frac{\gamma_2}{\sin\pi/6}\sin(\pi/6-\theta)\quad(0\le\theta\le\pi/6) \tag{2}$$

where γ_1 and γ_2 represent the edge energies along two principal directions (PDs),

and θ denotes the angular deviation from the most adjacent PD2, as shown in Fig. 1(c). Without loss of generality, we assume $\gamma_1 < \gamma_2$. For graphene, PD1 is armchair direction and PD2 is zig-zag direction. Although Eq. (2) only gives the edge energy for θ ranging from 0 to $\pi/6$, its extension to the whole spectrum of θ can be easily made based on the symmetry and periodicity of γ. In addition to graphene, transition metal dichalcogenides (TMDs) such as MoS_2 and PtS_2 are assumed to have fracture energy with similar direction dependence given by Eq. (2) because of their similar hexagonal lattice structure.

Griffith criterion in fracture mechanics [35,37] states that crack propagation happens when the energy release rate reaches the fracture energy. Therefore, the direction of crack propagation for a 2D material under tearing depends on the competition between G and 2γ, both of which are direction-dependent. With the increase of tearing load, crack propagation eventually takes place along the direction that the energy release rate reaches the corresponding fracture energy first. By comparing G and 2γ given by Eqs. (1) and (2), we find that the cracking direction of the graphene under tearing actually depends on $\alpha \equiv \theta - \phi$, which represents the misalignment between the tearing direction and the most adjacent PD2, as shown in Fig. 1(c). Specifically speaking, if $0 < \alpha_c < \alpha < \pi/6$, fracture tends to happen along PD1 ($\theta = \pi/6$); otherwise, if $0 < \alpha < \alpha_c < \pi/6$, fracture happens along PD2 ($\theta = 0$). Here, α_c is the critical tearing angle α given by [38]

$$\alpha_c = 2\tan^{-1}\left[2\sqrt{(2+\sqrt{3})\gamma_1/\gamma_2} - (2+\sqrt{3})\right]. \qquad (3)$$

When $\alpha = \alpha_c$, Griffith condition for crack propagation ($G = 2\gamma$) is meet along PD1 and PD2 simultaneously. The comparison between G and 2γ in this critical scenario is shown in Fig. 2(a) for the case with $\gamma_1/\gamma_2 = 0.95$. Such bifurcate proclivity of the cracking direction always exists if the ratio γ_1/γ_2 is greater than $\left(\sqrt{3}+2\right)/4 \approx 0.933$

as implied by Eq. (3). If $\gamma_1/\gamma_2 < 0.933$, Griffith condition for crack propagation is met only along PD1 irrespective of tearing angle α, as shown in Fig. 2(b) for the case with $\gamma_1/\gamma_2 = 0.92$. Under this circumstance, cracking occurs along PD1 only irrespective of the tearing direction. Such dependence of cracking direction on γ_1/γ_2 and α can be summarized by a map as shown in Fig. 2(c). In addition to graphene, above analysis and Fig. 2(c) may also apply to other 2D materials, such as MoS_2 and PtS_2, provided that their directional dependence of fracture energy obeys Eq. (2) with PD1 being the armchair or zig-zag direction, whichever is weaker in terms of edge energy. In real exfoliation experiments, however, the tearing angle α is uncontrollable and can be viewed as a random value ranging from 0 to $\pi/6$. Therefore, the probability of attaining cracking edges along PD2 is equal to the ratio of α_c over $\pi/6$, namely $6\alpha_c/\pi$. Similarly, the probability of attaining cracking edges along PD1 is $1-6\alpha_c/\pi$. For graphene, the edge energies along armchair (PD1) and zig-zag (PD2) are 1.03 eV/Å and 1.08 eV/Å, respectively [19], giving that $\gamma_1/\gamma_2 = 0.954$ and $\alpha_c = 0.083$ rad. Therefore, among all the fracture edges created by exfoliation, we can estimate that 15.9 % are zig-zag (PD2) and 84.1% are armchair (PD1). For MoS_2 and PtS_2, the ratios of γ_1/γ_2 are 0.843 and 0.717, respectively[25,38], both of which are less than 0.933. Fig. 2(c) implies that all the fracture edges are along PD 1, which is the zig-zag direction for both of them.

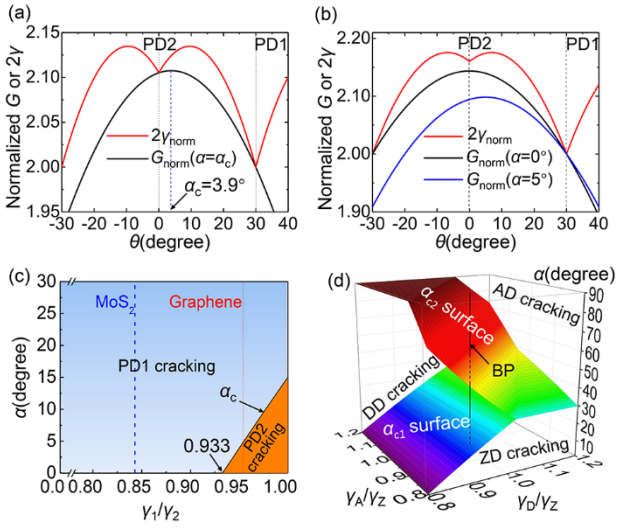

FIG. 2. Comparison of normalized ERR(G_{norm}) and fracture energy ($2\gamma_{\text{norm}}$) of hexagonal 2D material at the cracking moment for (a) $\gamma_1/\gamma_2 = 0.95$ and (b) $\gamma_1/\gamma_2 = 0.92$. Dependence of cracking direction on the tearing angle α and ratio of fracture energies along different principal directions for (c)hexagonal 2D materials and (d) orthorhombic 2D material.

For other 2D materials with crystallographic structures different from hexagonal one, above theoretical model is still applicable. But the principal directions and the directional dependence of edge energy might be different. Specifically, for BP, which is a typical orthorhombic 2D material, there are three types of principal direction: ZD (zig-zag direction <100>), AD (armchair direction <010>) and DD (diagonal direction <110>) [3,39-42], as shown in Fig. 1(d). Define tearing angle α as the misalignment between TD and the most adjacent ZD. Due to the $\pi/2$ periodicity of the BP lattice in the circumferential direction, α ranging from 0 to $\pi/2$ is considered. By comparing the ERR and the fracture energy[38], we find that if $0 < \alpha < \alpha_{c1}$, fracture happens along ZD; if $\alpha_{c1} < \alpha < \alpha_{c2}$, fracture happens along DD; if $\alpha_{c2} < \alpha < \pi/2$, fracture happens along AD. Here, α_{c1} and α_{c2} are two critical tearing angles[38]. The dependence of α_{c1} and α_{c2} on the edge energies of three principal directions is shown by Fig. 2(d). Assuming the tearing direction is random, for BP with $\gamma_A/\gamma_Z = 0.96$, $\gamma_D/\gamma_Z = 0.99$, we can estimate that among the fracture edges created by mechanical

exfoliation 29.3% are along ZD, 26.5% are along AD, and 44.2% are along DD.

Inter-edge angles of exfoliated flakes.—Although we have predicted the possible edge orientations of exfoliated 2D materials, verification by direct measurement is still hard because of the difficulty in determining the crystal orientation of 2D material edges in experiment. Therefore, a practical approach to verify the theoretical prediction is needed. Following our earlier work [18], inter-edge angles between any two straight edges on a flake [see Figs. 3(a)-3(b)] are measured and counted. For a flake with n straight edges, $n(n-1)/2$ inter-edge angles can be obtained. Since an inter-edge angle describes the relative orientation between two edges, its measurement can be easily made with an optical microscope. Meanwhile, the inter-edge angles obtained from different flakes can be integrated together for statistical analysis. Since the edges of the exfoliated flakes have preferred orientation, inter-edge angles must possess some regularity in statistics. In the following, we will first carry out a theoretical prediction of the statistic distribution of the inter-edge angles, followed by experimental verification.

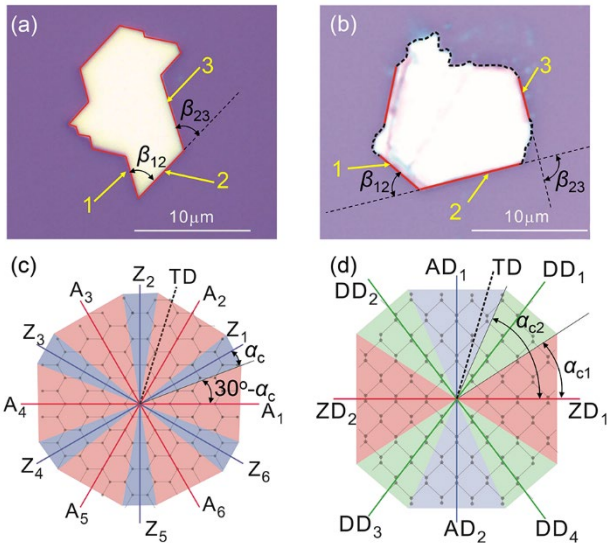

FIG. 3. Measurement of inter-edge angles from the optical microscope images of exfoliated flakes of (a) PtS_2(1T) (b) BP. Here, inter-edge angle is defined as the angle between any two straight edges that are not necessarily adjacent. If such measurement gives an angle exceeding

$\pi/2$, its supplementary angle will be adopted as the inter-edge angle. For two parallel edges, the inter-edge angle is 0. Schematics for inter-edge angle prediction of (c) hexagonal 2D material and (d) orthorhombic 2D material.

To quantitatively predict the inter-edge angles of 2D material flakes, all the principal directions in the plane should be distinguished, as shown in Figs. 3(c)-3(d). Taking graphene as an example, there are 6 armchair and 6 zig-zag directions labelled by A_i and Z_i (i =1, …, 6) [see Fig. 3(c)]. Based on above analysis, we can find out that if TD falls in the vicinity of any zig-zag direction as denoted by blue [see Fig. 3(c)], fracture will happen along that zig-zag direction. Similarly, if TD falls in the vicinity of any armchair diction as denoted by red [see Fig. 3(c)], fracture will happen along that armchair direction. Assuming that the TD is randomly distributed in the plane, the probabilities of cracking along a specific armchair or zig-zag direction can be expressed as

$$\begin{aligned} P(\mathrm{A}_i) &= 2(\pi/6-\alpha_c)/2\pi, \quad (i=1,\ldots,6) \\ P(\mathrm{Z}_i) &= 2\alpha_c/2\pi, \quad (i=1,\ldots,6) \end{aligned} \tag{4}$$

Eq. (4) is different from the probabilities of cracking along PD1 and PD2 as discussed in previous section because here different armchair (or zig-zag) directions are distinguishable.

For 2D materials with hexagonal lattice, our preceding analysis indicates that cracking happens along either PD1 or PD2. Considering the $\pi/3$ periodicity of PD1 and PD2 along circumferential direction, it is easy to deduce that there are four possible inter-edge angles for hexagonal 2D material flake: 0° (formed by two parallel edges), 30° (formed by PD1 and PD2), 60° (formed by two non-collinear PD1 or PD2) and 90° (formed by PD1 and PD2). The probability of acquiring inter-edge angle β is denoted as $P(\beta)$ and can be given as function of $P(\mathrm{A_i})$ and $P(\mathrm{Z_i})$[38]. For hexagonal 2D materials, $P(\beta)$ can be further expressed as a function of the ratio between two principal edge energies γ_1/γ_2 as shown in Fig. 4(a). According to their respective ratios of

γ_1/γ_2, one can easily find the positions of graphene, MoS_2 and PtS_2 in Fig. 4(a). For MoS_2 and PtS_2, $P(30^\circ)=P(90^\circ)=0$, $P(0^\circ)=1/3$, $P(60^\circ)=2/3$. Therefore, only two possible inter-edge angles (0° and 60°) can be observed from the flakes of MoS_2 and PtS_2, and the probability of 60° is about twice of that of 0°. For graphene, on the other hand, there are four possible inter-edge angles and the probabilities of having them are $P(0^\circ)=18.5\%$, $P(30^\circ)=29.7\%$, $P(60^\circ)=37.0\%$ and $P(90^\circ)=14.8\%$. Such difference in the statistic distribution of the inter-edge angles essentially can be attributed to the weaker anisotropy of fracture energy in graphene than those in MoS_2 and PtS_2. Therefore, the statistic distributions of inter-edge angles of exfoliated 2D materials are informative and can be used to predict the possible edge orientations.

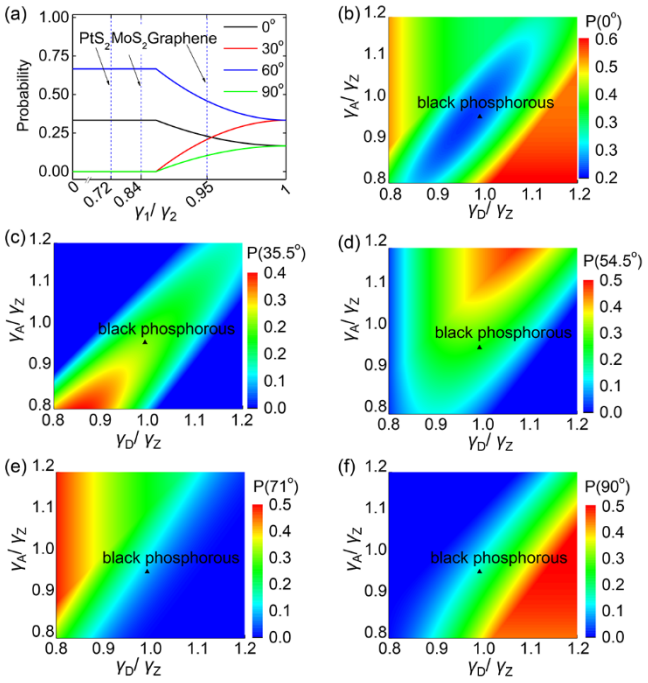

FIG. 4. (a)Probabilities of different inter-edge angles with respect to γ_1/γ_2 for hexagonal 2D materials. Probabilities of different inter-edge angles for black phosphorous with inter-edge angle being (b)0°, (c)35.5°, (d)54.5°, (e)71° and (f)90°.

For BP which has different crystallographic structure from hexagonal 2D materials [see Fig. 3(d)], similar analysis can also be carried out. Three PDs in BP give rise to 5 possible inter-edge angles: 0° (formed by two parallel edges), 35.5° (formed by AD and

DD), 54.5° (formed by ZD and DD), 71° (formed by two non-collinear DD) and 90° (formed by AD and ZD). The probabilities with these inter-edge angles can be expressed as functions of two ratios γ_A/γ_Z and γ_D/γ_Z (see Supplementary Material[38] for derivation), as shown in Figs. 4(b)-4(f). Taking $\gamma_A/\gamma_Z = 0.96$ and $\gamma_D/\gamma_Z = 0.99$ for BP[38], the probabilities of having these inter-edge angles can be determined from Figs. 4(b)-4(f). Specifically, $P(0^\circ) = 25.4\%$, $P(35.5^\circ) = 23.4\%$, $P(54.5^\circ) = 25.9\%$, $P(71^\circ) = 9.7\%$ and $P(90^\circ) = 15.6\%$.

Experimental verification.—To verify the above predictions, Inter-edge angles within the same 2D material flake are measured and counted. Data from different flakes are integrated, giving rise to sufficient counts for statistical analysis. Figs. 5(a)-5(d) show the histograms of the measured counts of inter-edge angles for graphene, MoS_2 (2H), PtS_2 (1T) and BP, respectively. For graphene, Fig. 5(a) shows four apparent peaks at 0°, 30°, 60° and 90°. For MoS_2 and PtS_2, peaks can be only observed at 0° and 60°, as shown in Fig. 5(b) and Fig. 5(c). We can thus deduce that fracture occurs either along PD1 or PD2 in graphene while always occurs along PD1(zig-zag direction) in MoS_2 and PtS_2. This finding agrees well with our theoretical prediction above. For BP, the peaks in Fig. 5(d) seem not as clear as those in Figs. 5(a)-5(c) except at 0° and 90°. A broad bump spanning from 30° to 75° is observed, which may be attributed to the interferences between the peaks at 35.5°, 54.5° and 71° as theoretically predicted above.

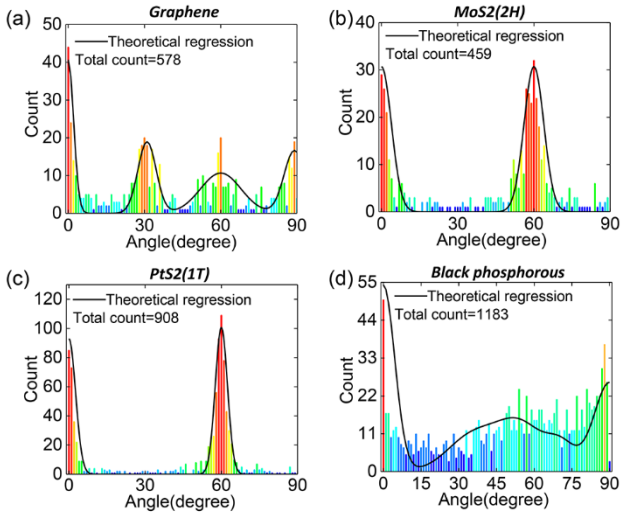

FIG. 5. Experimental statistics and corresponding theoretical regression for inter-edge angle distributions of (a)graphene (b) MoS_2 (2H) (c) PtS_2 (1T) and (d)black phosphorous.

Clearly, the distributions of the measured inter-edge angles are not as discrete as our theoretical prediction. This can be attributed to the unavoidable uncertainties in measurement including image distortion, sample defects, *etc*. To quantify these effects, statistical uncertainties of the measured inter-edge angles should be considered. Taking hexagonal 2D materials as an example, we assume that the measured inter-edge angles obey normal distributions with expectations of $0^\circ, 30^\circ, 60^\circ$ and 90°, respectively. The count of getting any inter-edge angles ω is given by

$$\begin{aligned} \mathrm{C}(\omega) = T \times [&2P(\beta_1)N\left(\beta_1, \sigma_{\beta_1}, \omega\right) + P(\beta_2)N\left(\beta_2, \sigma_{\beta_2}, \omega\right) \\ &+ P(\beta_3)N\left(\beta_3, \sigma_{\beta_3}, \omega\right) + 2P(\beta_4)N\left(\beta_4, \sigma_{\beta_4}, \omega\right)] \end{aligned} \tag{5}$$

where T is total count of the measurements, β_i (i=1, …, 4) stands for the expectation of inter-edge angle (i.e., $0^\circ, 30^\circ, 60^\circ$ or 90°), $N\left(\beta_i, \sigma_{\beta_i}, \omega\right)$ is the normal distribution function with β_i and σ_{β_i} being the expectation and standard deviation, respectively. For BP, the same method can be used with expectations of the inter-edge angle β_i (i=1, …, 5) being 0°, 35.5°, 54.5°, 71° and 90°, respectively. The count of any

inter-edge angles ω is given by:

$$\begin{aligned} \mathrm{C}(\omega) = T \times [2P(\beta_1)N(\beta_1, \sigma_{\beta_1}, \omega) + P(\beta_2)N(\beta_2, \sigma_{\beta_2}, \omega) \\ + P(\beta_3)N(\beta_3, \sigma_{\beta_3}, \omega) + P(\beta_4)N(\beta_4, \sigma_{\beta_4}, \omega) + 2P(\beta_5)N(\beta_5, \sigma_{\beta_5}, \omega)] \end{aligned} \quad (6)$$

In Eqs. (5) and (6), all the standard deviations σ_{β_i} are to be determined by regression from the experimental count distributions based on the least squares method[38]. After regression, the inter-edge angle distributions of Eqs. (5) and (6) are plotted using continuous solid curves in Fig. 5. It can be seen that Eq. (5) gives quite good theoretical predictions to the experimental histograms for all the hexagonal 2D materials under consideration. For BP, Fig. 5(d) shows that Eq. (6) describes the distribution of the measured inter-edge angles very well.

Conclusion.—In summary, we systematically investigate the fracture of 2D materials by mechanical exfoliation through theoretical modelling and experimental verification. We study a few representative 2D materials with different structures (hexagonal and orthorhombic) and anisotropic properties (graphene and TMDs). Our studies unambiguously reveal that the orientations of the fracture edges of exfoliated 2D materials exhibit a certain level of regularity, which is dependent on the tearing angle and anisotropy of fracture energy. Furthermore, the probabilities of the fracture occurring along these orientations are quantitatively predicted. We experimentally examine the inter-edge angles by optical microscopy and perform a statistical analysis. The experimental data show good agreement with our theoretical prediction and validate a general approach for interpreting the fracture behavior and the characteristics of flake edge of 2D materials. Our findings also provide useful guidance for the design and fabrication of 2D material based devices, especially for those with high anisotropy.

This work was supported by the Research Grant Council of Hong Kong (Grant No.: PolyU 152145/15E) and the Hong Kong Polytechnic University (Grant No.: G-

YBPS).

*ychai@polyu.edu.hk (YC), mmhyao@polyu.edu.hk(HY)

[1] A. K. Geim, Science **324**, 1530 (2009).
[2] G. R. Bhimanapati *et al.*, ACS Nano **9**, 11509 (2015).
[3] V. Sorkin, Y. Cai, Z. Ong, G. Zhang, and Y. W. Zhang, Critical Reviews in Solid State and Materials Sciences **42**, 1 (2017).
[4] K. Nakada, M. Fujita, G. Dresselhaus, and M. S. Dresselhaus, Physical Review B **54**, 17954 (1996).
[5] S. Z. Butler *et al.*, ACS Nano **7**, 2898 (2013).
[6] R. Mas Balleste, C. Gomez Navarro, J. Gomez Herrero, and F. Zamora, Nanoscale **3**, 20 (2011).
[7] V. Eswaraiah, Q. Zeng, Y. Long, and Z. Liu, Small **12**, 3480 (2016).
[8] G. Eda and M. Chhowalla, Nano Letters **9**, 814 (2009).
[9] Q. H. Wang, K. Kalantar-Zadeh, A. Kis, J. N. Coleman, and M. S. Strano, Nature Nanotechnology **7**, 699 (2012).
[10] Y. Zhao, J. Qiao, P. Yu, Z. Hu, Z. Lin, S. P. Lau, Z. Liu, W. Ji, and Y. Chai, Advanced Materials **28**, 2399 (2016).
[11] J. N. Coleman *et al.*, Science **331**, 568 (2011).
[12] J. Jeon, S. K. Jang, S. M. Jeon, G. Yoo, Y. H. Jang, J. H. Park, and S. Lee, Nanoscale **7**, 1688 (2015).
[13] X. Li *et al.*, Science **324**, 1312 (2009).
[14] K. Novoselov, D. Jiang, F. Schedin, T. Booth, V. Khotkevich, S. Morozov, and A. Geim, Proceedings of the National Academy of Sciences of the United States of America **102**, 10451 (2005).
[15] C. Virojanadara, M. Syväjarvi, R. Yakimova, L. I. Johansson, A. A. Zakharov, and T. Balasubramanian, Physical Review B **78**, 245403 (2008).
[16] Y. Huang, E. Sutter, N. N. Shi, J. Zheng, T. Yang, D. Englund, H. J. Gao, and P. Sutter, ACS Nano **9**, 10612 (2015).
[17] M. Yi and Z. Shen, Journal of Materials Chemistry A **3**, 11700 (2015).
[18] Y. Guo *et al.*, ACS Nano **10**, 8980 (2016).
[19] K. Kim, V. I. Artyukhov, W. Regan, Y. Liu, M. Crommie, B. I. Yakobson, and A. Zettl, Nano Letters **12**, 293 (2011).
[20] N. Kumar, S. Najmaei, Q. Cui, F. Ceballos, P. M. Ajayan, J. Lou, and H. Zhao, Physical Review B **87**, 161403 (2013).
[21] L. Liang, J. Wang, W. Lin, B. G. Sumpter, V. Meunier, and M. Pan, Nano Letters **14**, 6400 (2014).

[22] W. Wu *et al.*, Nature **514**, 470 (2014).
[23] W. Jin *et al.*, Physical Review B **91**, 121409 (2015).
[24] J. Zhang, J. Xiao, X. Meng, C. Monroe, Y. Huang, and J.-M. Zuo, Physical Review Letters **104**, 166805 (2010).
[25] S. Wang, Z. Qin, G. S. Jung, F. J. Martin-Martinez, K. Zhang, M. J. Buehler, and J. H. Warner, ACS nano **10**, 9831 (2016).
[26] P. Wagner, C. P. Ewels, V. V. Ivanovskaya, P. R. Briddon, A. Pateau, and B. Humbert, Physical Review B **84**, 134110 (2011).
[27] C. R. Zhu *et al.*, Physical Review B **88**, 121301 (2013).
[28] T. Mohiuddin *et al.*, Physical Review B **79**, 205433 (2009).
[29] E. F. Rauch and M. Véron, Materials Characterization **98**, 1 (2014).
[30] D. A. Chenet, O. B. Aslan, P. Y. Huang, C. Fan, A. M. van der Zande, T. F. Heinz, and J. C. Hone, Nano Letters **15**, 5667 (2015).
[31] Y. Li, Y. Rao, K. F. Mak, Y. You, S. Wang, C. R. Dean, and T. F. Heinz, Nano Letters **13**, 3329 (2013).
[32] L. Neeman, R. Ben-Zvi, K. Rechav, R. Popovitz-Biro, D. Oron, and E. Joselevich, Nano Letters **17**, 842 (2017).
[33] A. K. Geim and K. S. Novoselov, Nature Materials **6**, 183 (2007).
[34] Y. You, Z. Ni, T. Yu, and Z. Shen, Applied Physics Letters **93**, 163112 (2008).
[35] J. Chang, J. Q. Xu, and Y. Mutoh, Engineering Fracture Mechanics **73**, 1249 (2006).
[36] Y. Liu, A. Dobrinsky, and B. I. Yakobson, Physical Review Letters **105**, 235502 (2010).
[37] T. L. Anderson, *Fracture mechanics: fundamentals and applications* (CRC press, 2005).
[38] See Supplemental Material at [URL will be inserted by publisher] for the determination of critical tearing angle, edge energy of PtS2, probabilities of inter-edge angles and standard deviations of the distributions of these probabilities.
[39] A. Ramasubramaniam and A. R. Muniz, Physical Review B **90**, 085424 (2014).
[40] Y. Liu, F. Xu, Z. Zhang, E. S. Penev, and B. I. Yakobson, Nano Letters **14**, 6782 (2014).
[41] M. U. Farooq, A. Hashmi, and J. Hong, Scientific Reports **6**, 26300 (2016).
[42] W. Li, G. Zhang, and Y. Zhang, The Journal of Physical Chemistry C **118**, 22368 (2014).